Thermalization with a chemical potential from AdS spaces

Damián Galante[1] and Martin Schvellinger[2]

IFLP-CCT-La Plata, CONICET and
Departamento de Física, Universidad Nacional de La Plata.
Calle 49 y 115, C.C. 67, (1900) La Plata,
Buenos Aires, Argentina.

Abstract

The time-scale of thermalization in holographic dual models with a chemical potential in diverse number of dimensions is systematically investigated using the gauge/gravity duality. We consider a model with a thin-shell of charged dust collapsing from the boundary toward the bulk interior of asymptotically anti-de Sitter (AdS) spaces. In the outer region there is a Reissner-Nordström-AdS black hole (RNAdS-BH), while in the inner region there is an anti-de Sitter space. We consider renormalized geodesic lengths and minimal area surfaces as probes of thermalization, which in the dual quantum field theory (QFT) correspond to two-point functions and expectation values of Wilson loops, respectively. We show how the behavior of these extensive probes changes for charged black holes in comparison with Schwarzschild-AdS black holes (AdS-BH), for different values of the black hole mass and charge. The full range of values of the chemical potential over temperature ratio in the dual QFT is investigated. In all cases, the structure of the thermalization curves shares similar features with those obtained from the AdS-BH. On the other hand, there is an important difference in comparison with the AdS-BH: the thermalization times obtained from the renormalized geodesic lengths and the minimal area surfaces are larger for the RNAdS-BH, and they increase as the black hole charge increases.

[1] dagalante@gmail.com
[2] martin@fisica.unlp.edu.ar

Contents

1 Introduction

Quark gluon plasma (QGP) has become a subject of considerable interest after the results from RHIC and LHC experiments of heavy ion collisions, from where it is possible to draw the conclusion that the system behaves like an ideal fluid with a small shear viscosity over entropy density ratio (η/s) [1, 2, 3]. The crucial outcome is that the QGP is a strongly coupled system. Theoretical calculations assume that the system is in thermal equilibrium, and it is probed at momentum scales below the equilibrium temperature T, *i.e.* in the hydrodynamical regime of the plasma. A suitable approach to the dynamical description of strongly coupled systems is based on the AdS/CFT correspondence [4, 5, 6]. In this context, many investigations have been carried out after the seminal paper by Policastro, Son and Starinets, where they proposed a relation between the shear viscosity of the finite-temperature $\mathcal{N} = 4$ supersymmetric $SU(N)$ Yang-Mills (SYM) theory plasma, in the large N limit, at strong-coupling regime, and the absorption cross section of low-energy gravitons by a near-extremal black three-brane [7]. The $\mathcal{N} = 4$ SYM theory at finite temperature (just above the deconfinement transition temperature T_c) in the large N limit, qualitatively behaves like the strongly coupled QGP. This statement is based on a number of lattice QFT computations (for a recent review see [8]). The results of [7] were obtained within the supergravity limit. The first leading order string theory corrections to η/s of strongly coupled SYM plasmas have been computed in [9]. On the other hand, electrical charge transport properties of strongly coupled SYM plasmas have been thoroughly studied as well. These include the electrical conductivity, which was firstly computed in [10] within the supergravity limit, while its string theory corrections were obtained in [11, 12]. The first computation of photoemission rates in this context was done in [13] and their corresponding leading order string theory corrections were obtained in [14].

The way in which the actual heavy ion collision process is understood involves four basic stages. It begins with the *approach* regime, where two heavy ions move toward each other at relativistic velocities, with kinetic energies typically about 100 GeV/nucleon. Soon after, once the heavy ions collide, a part of their kinetic energies transforms into intense heat and the plasma of quarks and gluons starts forming. This is the *thermalization* process. After that, the strongly coupled QGP is formed, and here is where the hydrodynamical description holds. Elliptic flow has been observed in this regime, and it has been concluded that the system behaves like an ideal fluid, *i.e.* with very low η/s. At the end, the system expands and cools down, leading to the *hadronization* process. Since QGP in thermal equilibrium is strongly coupled, in principle, it is possible that the thermalization described above also occurs within a strongly coupled regime of QCD. Regardless of whether or not this hypothesis holds, it is very interesting to think about the thermalization of a strongly coupled system. In fact, in a series of papers the issue has been studied considering the collapse of a thin shell of matter, by using an AdS-Vaidya type metric [15, 16, 17, 18, 19, 20, 21, 22, 23, 24, 25, 26,

27]. Earlier studies of holographic thermalization described as a dual process of black hole formation have been presented in references [28, 29, 30, 31, 32, 33, 34, 35].

In a more realistic physical situation one should also consider the chemical potential, μ. Thus, it is very interesting to study the effect of the chemical potential on the thermalization time scale. This can be qualitatively modeled by a collapsing thin shell of charged matter, leading to a thermal equilibrium configuration given by a Reissner-Nordström-AdS black hole. In this paper we carry out a detailed systematic investigation, exploring the full range of the chemical potential/equilibrium temperature ratio, μ/T, in diverse number of dimensions, for both renormalized geodesic lengths and minimal area surfaces. In a real QGP the ratio μ/T is about 0.15 or less, thus the chemical potential effects will be limited [36, 37, 38, 39, 40]. For instance, at supergravity level, η/s remains the same with finite chemical potential. However, it is interesting to consider the effect of the chemical potential on the thermalization time scale for different holographic probes, mainly to be able to investigate the behavior of a collapsing shell of charged matter in AdS spaces. This may have applications to other physical systems beyond the context of SYM plasmas, such as certain condensed matter systems in two and three dimensions. We would like to emphasize that although the main motivation for the present work has been to consider thermalization of QGPs, which concerns RNAdS$_5$ black holes, the systematic exploration extended to lower and higher dimensions presented here would perhaps motivate further studies from the AdS/CMT perspective (for 3 and 4 dimensional backgrounds) as well as higher dimensional dual QFTs (corresponding to 6 and 7 dimensional backgrounds). It certainly will be of interest to investigate whether these effective backgrounds can be lifted to ten-dimensional string theory or eleven-dimensional M-theory descriptions, or at least to understand the difficulties to do it.

In section 2 we describe a model of holographic thermalization at strong coupling using two types of extensive geometric probes which are dual to two-point functions of QFT gauge invariant local operators and expectation values of rectangular Wilson loops. In section 3 we will describe the Reissner-Nordström-AdS black hole in arbitrary number of dimensions. There is an important reason to carry out a systematic study in different dimensions, which is the fact that the probes of thermalization such as renormalized geodesic lengths and minimal area surfaces are one- and two-dimensional geometric objects, respectively. Thus, by increasing the number of background spacetime dimensions, it allows to explore the ability of these extended objects to probe additional bulk degrees of freedom. This effect is significant as we will show from the figures introduced in the last section of the paper. We will introduce a time-dependent AdS-Vaidya type metric, including charged matter in the collapsing shell. This is essential for the present study of thermalization, and with it we will study thermalization of two-point functions of gauge invariant local operators in the dual conformal field theory (CFT), as well as rectangular Wilson loops, in the whole range $0 \leq \mu/T \leq \infty$. This is done for QFTs in 3, 4, 5 and 6 dimensions. In the case of AdS$_3$/CFT$_2$ duality there are charged extensions of the BTZ black hole [41], however

these are special cases that we shall not discuss here. Our results show that the effect of introducing chemical potential produces a delay in the thermalization time of the dual strongly coupled system. This effect indeed becomes more evident as the size of geometric probe increases. Our results are consistent with a top-down thermalization process, which was already observed in previous computations with no chemical potential [19, 18, 20], and is inherent to a strongly coupled computation. Thus, as it happens for the AdS-BH case, in the RNAdS-BH geometry UV modes thermalize first. This is a natural consequence of the setup of a collapsing thin shell, since smaller geodesics and smaller minimal area surfaces dual to Wilson loops thermalize before the corresponding larger probes do. It would be interesting to consider fat collapsing shells and see whether the top-down thermalization persists. Another observation from this systematic analysis is that, for sufficiently large probes, a swallow-tail like pattern appears in the thermalization curves, both for renormalized geodesic lengths and minimal area surfaces. This is a known effect in systems with two different relevant scales. We shall discuss about the relevance of these scales. On the other hand, this pattern could possibly be a consequence of a numerical artifact due to the fact that numerically we never have a shell with zero thickness. In addition, the swallow tails could appear from the breakdown to the probe approximation near the horizon, as it happens in top-down models when considering extremal probes instead of fundamental string probes including the thermalization of the string degrees of freedom [42]. After a detailed numerical analysis our conclusion is that the swallow tails are due to the emergence of certain solutions, from which only one is relevant for thermalization.

It is interesting to note the relation between two-point functions and expectation values of Wilson loops with the entanglement entropy in AdS_3 and AdS_4, respectively. Ryu and Takayanagi [43, 44, 45] proposed a way to calculate entanglement entropy holographically by considering minimal area surfaces in AdS spaces. Thus, by computing geodesics in AdS_3 and minimal area surfaces in AdS_4, we will also be computing the evolution of the entanglement entropy during the thermalization of CFTs in 2 and 3 dimensions, respectively, at finite temperature and finite chemical potential.

Finally, it is also interesting to note the differences in comparison with previous recent works. For a more complete description of investigations related to scenarios of thermalization of an initial field configuration far from equilibrium see [20] and references therein. In [19, 20] it is considered the thermalization from a collapsing shell of pressureless dust leading to Schwarzschild-AdS black holes in 3, 4 and 5 dimensions. The thermalization probes in these references are renormalized geodesic lengths, minimal area surfaces and minimal volumes. Then in [17] it is studied the evolution and scaling of the entanglement entropy for a 3 dimensional field theory using a thermal quench, leading to an asymptotically anti-de Sitter Schwarzschild black hole in four dimensions. In addition, they consider an electromagnetic quench, which after complete thermalization, renders an extremal dyonic black hole in four dimensions. In this reference the entanglement entropy is studied. More recently, in ref-

erence [24] thermalization following a non-relativistic quench near a quantum critical point with non-trivial dynamical critical exponent has been studied. They consider a collapsing shell leading to asymptotically Lifshitz spaces. In our present work we consider all cases for AdS_{d+1} spaces with d =3, 4, 5, and 6, exploring the full range of μ/T, considering different values of the boundary separation ℓ. We also study the swallow tails emerging from the thermalization curves, for renormalized geodesic lengths and minimal area surfaces. We also show explicitly the shape of geodesics corresponding to zero and finite chemical potential, for a given boundary separation ℓ, considering a set of different times. This allows to show graphically the actual shape evolution of the geodesics as the thin shell moves toward the bulk interior.

2 A model of holographic thermalization at strong coupling

In this section we describe a model of holographic thermalization of a strongly coupled CFT based on [19, 20]. We present a Vaidya-type metric where a thin shell of charged pressureless dust collapses to form a charged, asymptotically anti-de Sitter black hole. Then, we analyze two types of QFT operators: two-point functions of local gauge invariant operators and expectation values of rectangular Wilson loops, that will be used in the next sections as probes of holographic thermalization.

We will generalize the Vaidya metric, which was originally introduced by P.C. Vaidya in 1943 in order to study how the geometry of spacetime evolves in the presence of a massive star, which varies its mass due to the effect of radiation [46, 47]. In the present case, we consider $d+1$-dimensional metrics that are asymptotically AdS_{d+1}. Thus

$$ds^2 = \frac{1}{z^2}\left[-f(v,z)dv^2 - 2dz\ dv + d\mathbf{x}^2\right]\ , \tag{1}$$

where $f(v,z)$ can be an arbitrary function of v and z which approaches 1 as z goes to zero. The AdS radius, R, has been set to 1. The z-coordinate is the inverse of the radial coordinate, $z = R^2/r$, so the AdS boundary is at $z = 0$. In addition, $\mathbf{x}$ stands for coordinates at the boundary except the time, $\mathbf{x} = (x_1, \cdots, x_{d-1})$. In particular, if we choose $f(v,z) = 1 - m(v)z^d$ we will be considering a shell (with no charge) that collapses to form a Schwarzschild-AdS black hole. Moreover, we can extend this geometry to include charge by defining

$$f_{RN}(z,v) = 1 - m(v)z^d + q(v)^2 z^{2d-2}\ , \tag{2}$$

where the subindex stands for Reissner-Nordström black hole and the expression holds for $d \geq 3$.

This type of metric is a solution of the equations of motion of the action

$$S_{RN-Vaidya} = S_{EMAdS} + S_{ext}, \tag{3}$$

where S_{EMAdS} is the Einstein-Maxwell anti-de Sitter action

$$S_{EMAdS} = -\frac{1}{16\pi G^{(d+1)}} \int d^{d+1}x\sqrt{-g}\left[\mathcal{R} - F^2 + d(d-1)\right] , \tag{4}$$

where the negative cosmological constant is defined as $\Lambda = -\frac{d(d-1)}{2}$ and S_{ext} is an external action, whose energy-momentum tensor and current will be specified below.

From this action the resulting equations of motion are

$$R_{\mu\nu} - \frac{1}{2}g_{\mu\nu}(\mathcal{R} - 2\Lambda - F^2) - 2F_{\mu\lambda}F^{\lambda}_{\nu} = 8\pi G^{(d+1)}T^{(ext)}_{\mu\nu} , \tag{5}$$

$$\frac{1}{\sqrt{-g}}\partial_\rho\left(\sqrt{-g}F^{\rho\sigma}\right) = 8\pi G^{(d+1)}J^{\sigma}_{(ext)} . \tag{6}$$

The AdS-Vaidya type metric presented in Eqs.(1) and (2), together with an electromagnetic potential defined as

$$A_\mu = -\frac{1}{c}q(v)z^{d-2}\delta_{\mu v}, \tag{7}$$

with $c = \sqrt{\frac{2(d-2)}{d-1}}$, satisfy the above equations of motion provided that the external currents are

$$8\pi G^{(d+1)}T^{(ext)}_{\mu\nu} = z^{d-1}\left(\frac{(d-1)}{2}\dot{m}(v) - (d-1)z^{d-2}q(v)\dot{q}(v)\right)\delta_{\mu v}\delta_{\nu v} , \tag{8}$$

$$8\pi G^{(d+1)}J^{\sigma}_{(ext)} = \sqrt{\frac{(d-1)(d-2)}{2}}z^{d+1}\dot{q}(v)\delta^{\sigma z} , \tag{9}$$

where the dot stands for derivative with respect to coordinate v. Note that in the chargeless case, the energy-momentum tensor only depends on $\dot{m}(v)$ so it is immediate to check that the null energy conditions are satisfied provided that $m(v)$ is non-decreasing function of v. The charged case is more subtle since it depends on the specific choice of both $m(v)$ and $q(v)$.

The functions $m(v)$ and $q(v)$ model the change in the mass and charge of the black hole. In particular, if both $m(v) = M$ and $q(v) = Q$ are constants, then v is the usual Eddington-Finkelstein coordinate,

$$dv = dt - \frac{dz}{1 - M\ z^d + Q^2 z^{2d-2}} , \tag{10}$$

where t is the time. If we rewrite the metric in terms of t and z, then the AdS-Vaidya type metric corresponds to a charged black-brane type geometry,

$$ds^2 = \frac{1}{z^2}\left[-(1 - Mz^d + Q^2 z^{2d-2})dt^2 + \frac{dz^2}{1 - M\ z^d + Q^2 z^{2d-2}} + d\mathbf{x}^2\right] . \tag{11}$$

Again, for $Q = 0$, we obtain a black-brane solution with an event horizon at $r_h = 1/z_h = M^{1/d}$.

On the other hand, if $m(v) = q(v) = 0$ the change of variables becomes $dv = dt - dz$, being the metric the usual AdS_{d+1} one. Thus, if we choose $m(v) = M\,\theta(v)$ and $q(v) = Q\,\theta(v)$, with θ being the step function, we obtain a spacetime separated into two regions by a shell: for $v < 0$ it is an AdS_{d+1} spacetime, otherwise it will be a Reissner-Nordström-AdS black hole. At $v = 0$ we have a shell of zero thickness. Since we will carry out a numerical study it is convenient to consider smooth functions like

$$m(v) = \frac{M}{2}\left(1 + \tanh\frac{v}{v_0}\right), \tag{12}$$

$$q(v) = \frac{Q}{2}\left(1 + \tanh\frac{v}{v_0}\right), \tag{13}$$

where v_0 represents a finite shell thickness. In the limit $v_0 \to 0$ we recover the step function that represents a shock wave. In this limit case the null energy conditions are also satisfied, while in the finite thickness case the analysis has to be done with some care (see Appendix for a complete discussion on this).

Once we have a metric to model the rapid injection of energy that initiates the thermalization process on the dual QFT, we have to choose a set of extended observables in the bulk which allow to evaluate the evolution of the system. The initial condition is that the spacetime is AdS_{d+1}. Then, after certain time elapses, the system reaches the thermodynamical equilibrium, and the bulk becomes a Reissner-Nordström-AdS black hole. A RNAdS-Vaidya type metric interpolates between these two spaces, describing the time evolution of the system. In order to follow this evolution we have to probe the bulk by using extended geometric objects, which should be computed before and after the system reaches the thermodynamical equilibrium. However, it is easy to imagine that not any observable can be used as a probe of thermalization. One may ask what happens with the expectation values of one-point functions of gauge invariant operators, such as the energy-momentum tensor for instance. The problem is that these are local operators and, therefore, cannot give information on the thermalization process. So, clearly one needs to consider extended probes. A possibility is to study correlation functions of two local gauge invariant operators on the field theory side.

The AdS/CFT correspondence allows to understand intuitively why the expectation values of local quantum field theory operators are insensible to the details of the thermalization. These observables can only account for effects due to bulk properties close to the AdS boundary, thus they do not allow to probe details from distances of the order of the thermal scale of the system. On the other hand, two-point functions of local gauge invariant QFT operators probe the bulk interior. Indeed, the AdS/CFT correspondence provides an elegant geometric way to compute two-point functions: under certain approximations the two-point functions correspond to geodesics which connect the two points where the local QFT operators are

inserted at the AdS boundary. These geodesics extend toward the bulk, thus allowing to probe a larger range of energies from the boundary field theory perspective. There are also other operators which are useful for the present problem: expectation values of Wilson loops which correspond to minimal area surfaces in the AdS bulk, as well as the entanglement entropy which is related to minimal volumes.

Following [20] we first consider two-point functions of local gauge invariant QFT operators at constant time as probes of thermalization. In general Wightman functions are defined as [19, 20]

$$G^{>}_{\mathcal{O}}(t,\mathbf{x};t',\mathbf{x}') =< \mathcal{O}(t,\mathbf{x})\mathcal{O}(t',\mathbf{x}') > , \tag{14}$$

where $\mathcal{O}$ is a local gauge invariant QFT operator of conformal dimension Δ. In order to follow the evolution of these functions we are interested in the equal time ($t = t'$) correlators. Then, we want to see how these functions vary at different times. When we consider strongly coupled QFTs these functions can only be computed analytically for dimension two. For higher dimensions the analytical treatment is unknown.

Fortunately, the AdS/CFT correspondence allows to evaluate these functions when the operators are heavy by using geodesics in AdS spaces. As it is well-known from the AdS/CFT dictionary a scalar field $\varphi(z,t,\mathbf{x})$ with mass m in $d+1$ dimensions is dual to an operator $\mathcal{O}$ whose conformal dimension is $\Delta = \frac{1}{2}(d+\sqrt{d^2+m^2})$. In general, the two-point function (14) in the strongly coupled regime is computed using the classical supergravity action in terms of φ. However, for our purpose it will be more convenient to compute it from a path integral as in reference [48, 20]

$$< \mathcal{O}(t,\mathbf{x})\mathcal{O}(t,\mathbf{x}') >= \int \mathcal{D}\mathcal{P} e^{i\Delta L(\mathcal{P})} \approx \sum_{\text{geodesics}} e^{-\Delta\mathcal{L}} , \tag{15}$$

where the path integral includes all possible paths connecting the points at the AdS boundary, *i.e.* $(t,\mathbf{x})$ and $(t,\mathbf{x}')$. In addition, $L(\mathcal{P})$ is the proper length corresponding to this path. For space-like trajectories $L(\mathcal{P})$ is imaginary. Thus, it is possible to make a saddle-point approximation for $\Delta \gg 1$. Therefore, only trajectories with extreme geodesic lengths will contribute. Notice that in the last term $\mathcal{L}$ indicates actual length of the geodesic between the points at the AdS boundary. In this way, there is a direct relation between the logarithm of the equal-time two-point function and the geodesic length between these two points. It is important to be careful while considering these approximations because the geodesic length diverges due to the AdS boundary contributions. Then, one can define a renormalized distance $\delta\mathcal{L} \equiv \mathcal{L} - 2\ln(2/z_0)$, in terms of the cut-off z_0. This suppresses the divergent part in the pure AdS.

The other type of non-local operators that we will be using are spatial Wilson loops, which are non-local gauge invariant operators in the field theory defined as the integral in a closed

path C of the gauge field

$$W(C) = \frac{1}{N} Tr \left(\mathcal{P} e^{\oint_C A} \right) , \tag{16}$$

where $\mathcal{P}$ means ordered product, N is the number of colors of the gauge theory, and A_μ is the non-Abelian gauge field. Wilson loops provide information about the non-perturbative behavior of gauge theories, however, in general it is difficult to compute them. Using the AdS/CFT correspondence its computation can be done in an elegant way. The expectation value of a Wilson loop is related to the string theory partition function with a world sheet Σ extended on the interior of the bulk, and ending on the closed contour C on the boundary,

$$< W(C) >= \int \mathcal{D}\Sigma e^{-\Lambda(\Sigma)} , \tag{17}$$

where one has to integrate over all the non-equivalent surfaces whose boundary is $\partial\Sigma = C$, at the AdS boundary. $\Lambda(\Sigma)$ is the string action. In the strong coupling regime we can carry out a saddle-point approximation of the string theory partition function. In this way we can reduce the computation of the expectation value of a Wilson loop to determine the surface of minimal area of the classical world-sheet whose boundary is C. Thus, can write

$$< W(C) > \simeq e^{-\frac{1}{\alpha'} \mathcal{A}(\Sigma_0)} , \tag{18}$$

where $\mathcal{A}(\Sigma_0)$ represents the area of the minimal surface. This will be a solution to the equations of motion of the bosonic part of the string action [52, 53].

These models based on the AdS/CFT correspondence allow to understand intuitively how the thermalization process takes place. Let us consider the sudden injection of energy in the dual QFT. The bulk geometry associated with this process is proposed to be described by a collapsing shell from the boundary toward the bulk interior. As long as the shell collapses, the outer region is described by a Reissner-Nordström-AdS black hole, while the inner region is still an AdS space. Now, let us use the geodesic approximation to compute the equal-time two-point functions. If the separation of the boundary points is small enough, then the geodesic cannot reach the shell at $v = 0$ and, therefore, the geodesic is seen as a purely RNAdS-BH geodesic, *i.e.* for short distances in the field theory the system seems to be in thermal equilibrium. If we increase the separation between the insertion of the boundary operators, at some point, the geodesic will cross the shell, and there will be a geodesic refraction which will deviate the geodesic in comparison with the thermal one. Thus, we can understand why the thermalization proceeds from short to long distances, *i.e.* QFT ultraviolet degrees of freedom thermalize first [20].

3 The Reissner-Nordström-AdS black hole

Let us now consider the pure Einstein-Maxwell anti-de Sitter action (with no external fields) which describes a $d+1$-dimensional space-time, with negative cosmological constant $\Lambda =$

$-\frac{d(d-1)}{2R^2}$, coupled to an Abelian gauge field A_M, with $M = 0, \cdots, d$ [49, 50]

$$S_{EMAdS} = -\frac{1}{16\pi G^{d+1}} \int d^{d+1}x\sqrt{-g}\left[\mathcal{R} - F^2 + \frac{d(d-1)}{R^2}\right] . \tag{19}$$

This action has been introduced in Section 2, however here we recover the AdS radius R. The solution to the equations of motion derived from the above action leads to the Reissner-Nordström-AdS black hole metric, which can be written in static coordinates as

$$ds^2 = -V(r)dt^2 + \frac{dr^2}{V(r)} + r^2 d\Omega^2_{d-1} , \tag{20}$$

where $d\Omega^2_{d-1}$ is the metric on the sphere S^{d-1}, and

$$V(r) = 1 + \frac{r^2}{R^2} - \frac{M}{r^{d-2}} + \frac{Q^2}{r^{2d-4}} . \tag{21}$$

In this metric M and Q are related to the ADM black hole mass $\bar{M}$ and the $\bar{Q}$ charge [51] as follows

$$\bar{M} = \frac{(d-1)\omega_{d-1}}{16\pi G} M , \tag{22}$$

$$\bar{Q} = \sqrt{2(d-1)(d-2)}\left(\frac{\omega_{d-1}}{8\pi G}\right) Q , \tag{23}$$

where ω_{d-1} is the volume of the unit radius sphere S^{d-1}. Also, there is a pure electrical gauge potential given by

$$A = \left(-\frac{1}{c}\frac{Q}{r^{d-2}} + \Phi\right) dt , \tag{24}$$

where $c = \sqrt{\frac{2(d-2)}{d-1}}$, while Φ is a constant which plays the role of the electrostatic potential in the region between the event horizon and the boundary of the asymptotic AdS. It is defined such that $A_t(r_h) = 0$. Thus,

$$\Phi = \frac{1}{c}\frac{Q}{r_h^{d-2}} . \tag{25}$$

Following [49] we can consider the limit where the boundary of AdS_{d+1} is $\mathbb{R}^d$ instead of $\mathbb{R} \times S^{d-1}$, the so-called infinite volume limit, which is important for the dual field theory discussion. This relays upon the presence of a negative cosmological constant. This limit can be obtained by introducing a dimensionless parameter λ, and set for the radial coordinate $r \to \lambda^{1/d} r$, for time coordinate $t \to \lambda^{-1/d} t$, for the mass and charge $m \to \lambda m$ and $q \to$

$\lambda^{(d-1)/d}q$, respectively, and for S^{d-1} we set $R^2 d\Omega_{d-1}^2 \to \lambda^{-2/d}\sum_{i=1}^{d-1} dx_i^2$. Then, if we consider the limit $\lambda \to \infty$, the metric becomes

$$ds^2 = -U(r)dt^2 + \frac{dr^2}{U(r)} + \frac{r^2}{R^2}\sum_{i=1}^{d-1} dx_i^2\,, \tag{26}$$

where

$$U(r) = \frac{r^2}{R^2} - \frac{M}{r^{d-2}} + \frac{Q^2}{r^{2d-4}}\,. \tag{27}$$

Notice that replacing r by $1/z$ (setting $R = 1$) in Eqs.(26) and (27) we obtain Eq.(11).

Using the gauge/gravity duality dictionary the Hawking temperature corresponding to a black hole is assumed to be the equilibrium temperature of the dual QFT. For the RNAdS-BH metric the temperature is given by

$$\beta_{RN} = \frac{1}{T_{RN}} = \frac{4\pi R^2}{dr_h - \frac{(d-2)Q^2R^2}{r_h^{2d-3}}}\,, \tag{28}$$

in terms of the black hole event horizon r_h and its charge parameter Q. This expression results from the usual procedure of demanding regularity at the event horizon of the Euclidean continuation of the metric. When $Q = 0$ this equation leads to $\beta = \frac{4\pi R^2}{dr_h}$, being the well-known Hawking temperature in the AdS-BH case. Then, for instance, setting $d = 4$ it reduces to the Hawking temperature of the Reissner-Nordström AdS_5 black hole [40],

$$\beta_{RN} = \frac{1}{T_{RN}} = \frac{\pi R^2}{r_h(1 - \frac{Q^2R^2}{2r_h^6})}\,. \tag{29}$$

We can also consider the black hole mass parameter in terms of the radius of the event horizon

$$M = \frac{r_h^d}{R^2} + \frac{Q^2}{r_h^{d-2}}\,. \tag{30}$$

We should notice that the RNAdS black hole has an extremal solution corresponding to $T = 0$. However, it nevertheless has an event horizon. This can be seen from Eq.(28), leading to

$$r_h|_{ext} = \left(\frac{(d-2)}{d}Q^2R^2\right)^{\frac{1}{2d-2}}\,. \tag{31}$$

This is a remarkable difference with respect to the Schwarzschild-AdS case, where the extremal solution corresponds to an anti-de Sitter spacetime. Another important difference

is that from the AdS/CFT correspondence it is possible to understand the electromagnetic field in this geometry as a source of the chemical potential in the dual quantum field theory. However, the precise relation is somehow subtle since the chemical potential has energy units in the dual field theory ($[\mu] = 1/[L]$) [40]. On the other hand, A_μ as defined in the action (19) is dimensionless, thus one has to redefine this field as $\bar{A}_\mu = A_\mu/R_*$, where R_* is a scale with length units. Therefore, $\bar{A}$ and μ have the same units. The only effect of this field redefinition is to change the Maxwell term in the action, changing the coupling as $g^2_{YM} = 4\pi G/R^2_*$. This is useful now because in this way we can obtain the chemical potential in the QFT as the boundary value of the time component of the bulk gauge field. Thus, we obtain

$$\mu = \lim_{r\to\infty} \bar{A}_t = \frac{\Phi}{R_*} = \frac{1}{c}\frac{Q}{r_h^{d-2} R_*}\,. \tag{32}$$

Therefore, the black hole charge is related to the chemical potential in the gauge theory. R_* depends on the particular compactification, whenever the solution could be obtained from string theory or M-theory. Besides the specific value of R_*, it is possible to study the whole range of values of μ/T given by

$$\frac{\mu}{T} = \frac{4\pi\, R^2\, Q}{c\, R_* \left(d\, r_h^{d-1} - \frac{(d-2)Q^2R^2}{r_h^{d-1}}\right)}\,. \tag{33}$$

Thus, if the radius of the event horizon r_h is kept fixed, then Eqs.(31) and (32) show that it is possible to go from $\mu/T = 0$, for $Q = 0$, to the extremal case, where $\mu/T \to \infty$, provided that Q satisfies Eq.(31). Recall that the mass is given by Eq.(30).

4 Holographic thermalization with a chemical potential

In this section we consider how the thermalization process occurs within the model described here. For this purpose we will study two-point functions of local gauge invariant operators and expectation values of rectangular Wilson loops in the dual conformal field theory. The former ones correspond to geodesic lengths in the bulk theory, while the second ones correspond to minimal area surfaces in the bulk. The idea is that we start from an anti-de Sitter spacetime of dimension $d + 1$. This is the holographic dual of the strongly coupled regime of a conformal field theory at zero temperature and zero chemical potential. Then, we consider a thin shell of charged dust propagating from the boundary toward the bulk interior, and collapsing, leading to a RNAdS black hole. From the dual QFT point of view this corresponds to a sudden injection of energy and matter, both modeled through holographic quenches, such that whenever the thermodynamical equilibrium is reached, the system will

be described within the grand canonical ensemble. As the thin shell of charged matter collapses in the bulk, it separates two regions. The outer one is a Reissner-Nordström black hole which is asymptotically AdS. The inner region is just an AdS spacetime.

This situation is described by a dynamical metric, which is the RNAdS Vaidya type metric given in Eqs.(1) and (2), using the functional forms of the mass and charge of Eqs.(12) and (13). The conjecture is that from the holographic dual field theory this dynamical situation corresponds to the thermalization process of a strongly coupled system. We will see that the holographic thermalization is a top-down process in the sense that UV degrees of freedom equilibrate first.

Now, we can actually calculate the geodesic length and the minimal area surface of the string attached to the boundary, as probes of thermalization for this geometry.

4.1 Renormalized geodesic lengths

We will be evaluating geodesic distances as function of both time and boundary separation length, in arbitrary number of spacetime dimensions. We will consider space-like geodesics between points $(t, x_1) = (t_0, -\ell/2)$ and $(t', x_1') = (t_0, \ell/2)$ in the case of $\mathrm{AdS}_3/\mathrm{CFT}_2$, where ℓ is the separation of the AdS boundary points. For $d = 3, 4, 5, 6$, the orthogonal coordinates are fixed. For instance, for $d = 4$ we have $(x_2, x_3) = (x_2', x_3')$. Thus, we take as the geodesic parameter the first coordinate x_1, which, in order to make simpler the notation, we rename as x. The solutions to the geodesic equations are given by the functions $v(x)$ and $z(x)$. Inserting a cut-off z_0 close to the AdS boundary, the boundary conditions become

$$z(-\ell/2) = z_0\,, \qquad z(\ell/2) = z_0\,, \qquad v(-\ell/2) = t_0\,, \qquad v(\ell/2) = t_0\,. \tag{34}$$

Also, $v(x)$ and $z(x)$ are symmetric under reflection $x \to -x$. The geodesic length is defined as

$$\mathcal{L} = \int \sqrt{-ds^2} = \int_{-\ell/2}^{\ell/2} dx \frac{\sqrt{1 - 2z'(x)v'(x) - f_{RN}(v,z)v'(x)^2}}{z(x)}\,, \tag{35}$$

where $f_{RN}(v, z)$ was defined in Eq.(2). The prime indicates derivative with respect to x. The functions $v(x)$ and $z(x)$ minimize the geodesic length of Eq.(35), thus the problem is similar to the one in classical mechanics with the same Lagrangian. Since the Lagrangian does not depend explicitly on x, there is one conserved quantity, equivalent to the Hamiltonian of the system. In terms of $f_{RN}(v, z)$ it becomes

$$\mathcal{H} = \frac{1}{z(x)\sqrt{1 - 2z'(x)v'(x) - f_{RN}(v,z)v'(x)^2}}\,. \tag{36}$$

Introducing the initial conditions on the tip of the geodesic as

$$z(0) = z_*\,, \qquad v(0) = v_*\,, \qquad v'(0) = z'(0) = 0\,, \tag{37}$$

the conservation equation simplifies to

$$1 - 2z'v' - f_{RN}(z,v)v'^2 = \left(\frac{z_*}{z}\right)^2 . \tag{38}$$

The next step is to compute the equations of motion for $v(x)$ and $z(x)$. Though in principle they have a complex form, it is possible to simplify them by making use of the conservation equation. In particular, we can differentiate Eq.(38) with respect to x and obtain a relation for $v''(x)$ and $z''(x)$. Inserting these relations in the equations of motion, we obtain a set of simplified, second order differential equations for $v(x)$ and $z(x)$ as follows

$$0 = 2 - 2v'(x)^2 f_{RN}(v,z) - 4v'(x)z'(x) - 2z(x)v''(x) + z(x)v'(x)^2\partial_z f_{RN}(v,z)\,, \tag{39}$$

which is obtained from the equation of motion for $z(x)$, while

$$\begin{aligned} 0 &= z(x)v''(x)f_{RN}(v,z) + z(x)z''(x) + z(x)z'(x)v'(x)\partial_z f_{RN}(v,z) \\ &\quad + \frac{1}{2}z(x)v'(x)^2\partial_v f_{RN}(v,z)\,, \end{aligned} \tag{40}$$

is obtained from the equation of motion of $v(x)$. From this set of equations (plus the initial values) we can numerically obtain $z(x)$ and $v(x)$ for each pair of v_* and z_*. We can also obtain the equations of motion in terms of m and q, just by replacing f_{RN} and its derivatives into Eqs.(39) and (40), leading to

$$\begin{aligned} 0 &= \frac{1}{2}d\, z(x)^d v'(x)^2 m(v) - z(x)^d v'(x)^2 m(v) - d\, z(x)^{2d-2}v'(x)^2 q(v)^2 \\ &\quad + 2z(x)^{2d-2}v'(x)^2 q(v)^2 + z(x)v''(x) + 2v'(x)z'(x) + v'(x)^2 - 1\,, \end{aligned} \tag{41}$$

$$\begin{aligned} 0 &= -\frac{1}{2}z(x)^d v'(x)^2 m'(v) - z(x)^d v''(x)m(v) - d\, z(x)^{d-1}v'(x)z'(x)m(v) \\ &\quad + z(x)^{2d-2}v'(x)^2 q(v)q'(v) + z(x)^{2d-2}v''(x)q(v)^2 + 2d\, z(x)^{2d-3}v'(x)z'(x)q(v)^2 \\ &\quad - 2z(x)^{2d-3}v'(x)z'(x)q(v)^2 + v''(x) + z''(x)\,, \end{aligned} \tag{42}$$

where the dot stands for partial derivative with respect to v.

The advantage of calculating the equations of motion in terms of $f_{RN}(v,z)$ is that they can be easily generalized to any other metric with that form. We can also obtain the equations of motion for the Schwarzschild-AdS case simply by changing $f_{RN}(v,z)$ for $f(v,z) = 1 - m(v)z^d$, *i.e.* setting $q(v) = 0$. It leads to the equations for geodesic lengths presented in [20], which is a consistency check for our calculations and it also allows to compare the RNAdS-BH with the Schwarzschild-AdS one.

At the end we are interested in evaluating the geodesic length in terms of time t_0 and the boundary separation ℓ. This information is given by

$$z(\ell/2) = z_0\,, \qquad\qquad v(\ell/2) = t_0\,. \tag{43}$$

By using the conservation equation and reflection symmetry we can easily calculate the on-shell geodesic length as

$$\mathcal{L}(\ell, t_0) = 2\int_0^{\ell/2} dx \frac{z_*}{z(x)^2}\,, \tag{44}$$

and subtract the divergent part defining $\delta\mathcal{L}(\ell, t_0) = \mathcal{L}(\ell, t_0) - 2\ln(2/z_0)$.

Thus, we can calculate how the thermalization process occurs by considering a collapsing thin shell of charged dust. It is interesting to compare these results with those obtained in the case of a collapsing thin shell of dust with no charge, such as those described in [20].

In order to study the thermalization we first have to see the evolution of the geodesics as shown in Fig. 1. Thus, we solve the problem for a metric with an event horizon located at $r_h = 1/z_h = 1$. The difference in comparison with the AdS-BH case is that now we have to set a non-vanishing charge/mass ratio. Let us consider $Q/M = 1/2$. This choice satisfies the restrictions from Eqs.(30) and (31). From Fig. 1 we can see and compare the evolution of geodesics with both a thin shell of charged and uncharged matter for $d = 4$. In both systems there is a similar behavior. For short times the geodesics do not change with respect to the pure AdS space. On the other hand, starting from $t_0 \sim 0.8$, in this configuration with operator boundary separation $\ell = 2.6$, differences between the charged and uncharged systems become apparent. Notice that within the range $0.8 < t_0 \leq 1$ geodesics in both systems change abruptly before both systems reach the thermodynamical equilibrium. Although this process is the same for the RNAdS-BH case, the actual evolution of the probes is different. Indeed, we notice differences which render the charged system to have a slightly larger thermalization time in comparison with the system at zero chemical potential.

4.2 Minimal area surfaces

We now focus on the thermalization of expectation values of rectangular Wilson loops. Proceeding in a similar way as for the geodesic lengths, now we consider the computation of the minimal area surfaces as described before. Using the AdS-Vaidya type metric, the Nambu-Goto action becomes,

$$\mathcal{A}_{NG}(t_0, \ell, R) = \frac{R}{2\pi}\int_{-\ell/2}^{\ell/2} dx \frac{\sqrt{1 - f_{RN}(v,z)v'^2 - 2z'v'}}{z^2}\,. \tag{45}$$

We are considering boundary rectangles parametrized by the coordinates (x_1, x_2). The rest of the coordinates (if there is any) at the AdS boundary are kept fixed. One assumes the translational invariance along x_2, thus, we will use x_1 to parametrize the functions $v(x_1)$

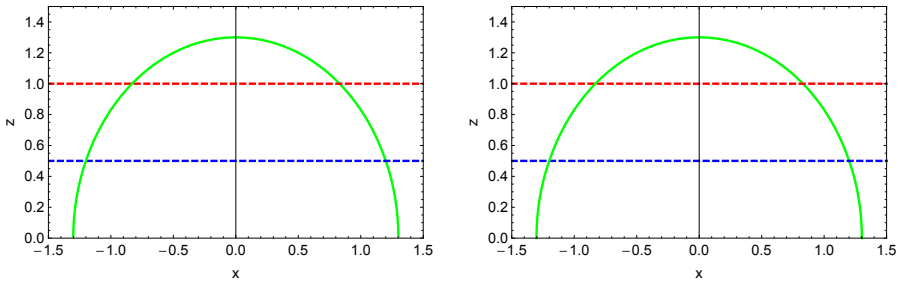

(a) $t_0 = 0.498$ - AdS-Vaidya

(b) $t_0 = 0.498$ - RNAdS Vaidya

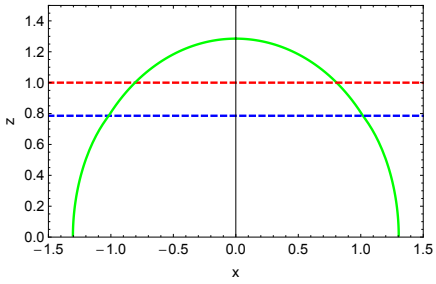

(c) $t_0 = 0.778$ - AdS-Vaidya

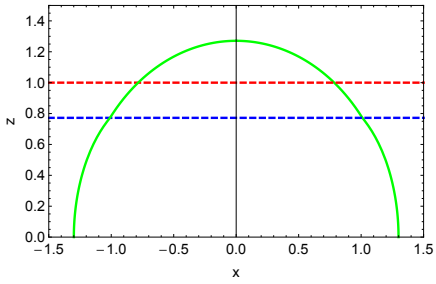

(d) $t_0 = 0.771$ - RNAdS Vaidya

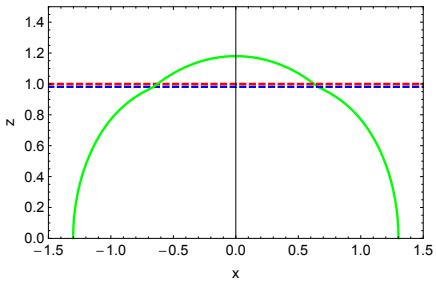

(e) $t_0 = 1.010$ - AdS-Vaidya

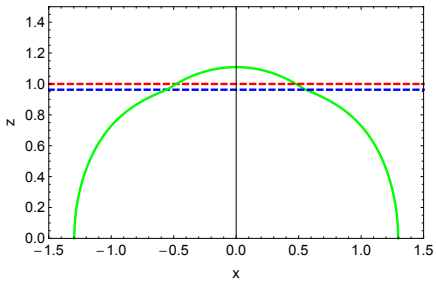

(f) $t_0 = 1.011$ - RNAdS Vaidya

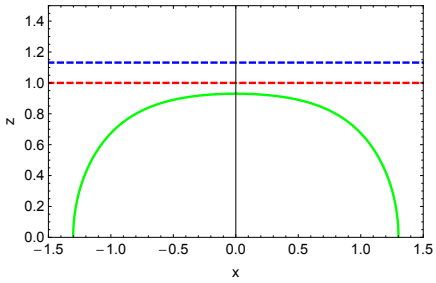

(g) $t_0 = 2.004$ - AdS-Vaidya

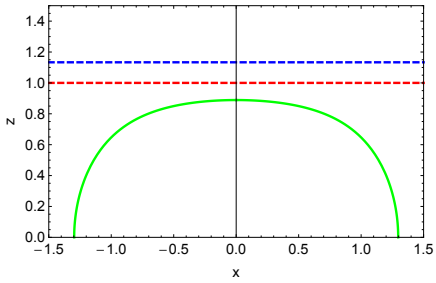

(h) $t_0 = 2.022$ - RNAdS Vaidya

Figure 1: Evolution of the shell of dust described by the AdS-Vaidya metric with $r_h = 1$, compared with a shell of charged dust described by the RNAdS Vaidya type metric also with $r_h = 1$ and $Q/M = 1/2$. In both cases the separation of the boundary field theory operator pair is $\ell = 2.6$. The black hole horizon is indicated by a dashed horizontal red line. The horizonal dashed blue lines indicate the position of the shell in each case. The time differences in each pair of figures is due to the fact that they have been obtained numerically, and therefore, there are minor differences.

and $z(x_1)$ in the AdS_{d+1}, and we call it x. Along the x_2 direction the rectangular path on the boundary has length R_{WL}.

As in the previous case, there is no explicit dependence on x and therefore, there is a conserved quantity corresponding to the Hamiltonian. The tip of the rectangular Wilson loop is z_*, with $z'(0) = v'(0) = 0$. Then, the conservation equation becomes

$$1 - 2z'v' - f_{RN}(v,z)v'^2 = \left(\frac{z_*}{z}\right)^4 . \tag{46}$$

The boundary conditions continue to be the same as in the geodesics case,

$$z(-\ell/2) = z_0\,, \qquad z(\ell/2) = z_0\,, \qquad v(-\ell/2) = t_0\,, \qquad v(\ell/2) = t_0\,. \tag{47}$$

Next, we have to minimize the Nambu-Goto action for this geometry. Since the calculations are similar to those for the two-point functions we will just focus on the final resulting expressions. The simplified equations of motion of $z(x)$ and $v(x)$ are respectively

$$0 = z(x)v'(x)^2\partial_z f_{RN}(v,z) - 4v'(x)^2 f_{RN}(v,z) - 2z(x)v''(x) - 8v'(x)z'(x) + 4\,, \tag{48}$$

$$0 = v'(x)z'(x)\partial_z f_{RN}(v,z) + \frac{1}{2}v'(x)^2\partial_v f_{RN}(v,z) + v''(x)f_{RN}(v,z) + z''(x)\,. \tag{49}$$

Using the explicit form of $f_{RN}(v,z)$ we obtain the following set of differential equations

$$\begin{aligned} 0 = {} & 4z(x)^d m(v)v'(x)^2 - 4z(x)^{2d-2}q(v)^2v'(x)^2 - 2z(x)v''(x) \\ & -8v'(x)z'(x) - 4v'(x)^2 + 4\,, \end{aligned} \tag{50}$$

$$\begin{aligned} 0 = {} & \frac{1}{2}z(x)^d v'(x)^2 m'(v) + z(x)^d m(v)v''(x) + dz(x)^{d-1}m(v)v'(x)z'(x) \\ & -z(x)^{2d-2}q(v)v'(x)^2q'(v) - z(x)^{2d-2}q(v)^2v''(x) - 2dz(x)^{2d-3}q(v)^2v'(x)z'(x) \\ & +2z(x)^{2d-3}q(v)^2v'(x)z'(x) - v''(x) - z''(x)\,, \end{aligned} \tag{51}$$

for $z(x)$ and $v(x)$, respectively, which we will solved numerically. These equations reduce to the corresponding ones presented in [20] when the charge is set to zero.

We can again extract the information of time and boundary separation length from

$$z(\ell/2) = z_0\,, \qquad\qquad v(\ell/2) = t_0\,, \tag{52}$$

and rewrite the on-shell Nambu-Goto action by making use of the conservation equation, obtaining

$$\mathcal{A}(t_0,\ell,R_{WL}) = \frac{R_{WL}}{\pi}\int_0^{\ell/2} dx\,\frac{z_*^2}{z^4}\,. \tag{53}$$

Finally, we subtract the divergent part from pure AdS space by defining

$$\delta\mathcal{A}(t_0,\ell,R_{WL}) = \mathcal{A}(t_0,\ell,R_{WL}) - \frac{1}{z_0}\frac{R_{WL}}{\pi}\,. \tag{54}$$

4.3 Evolution of thermalization probes

Having the information about the geodesic lengths and minimal area surfaces as a function of time, we can describe the thermalization process. In order to do it we compare $\delta\mathcal{L}$ and $\delta\mathcal{A}$ at each time with the final values $\delta\mathcal{L}_{RN}$ and $\delta\mathcal{A}_{RN}$, obtained in the pure Reissner-Nordström-AdS black hole geometry, *i.e.* by setting both $m(v) = M$ and $q(v) = Q$ constant. This procedure is repeated for different AdS-boundary separations ℓ and different spacetime dimensions. We prefer to plot the quantities $\delta\bar{\mathcal{L}} \equiv \delta\mathcal{L}/\ell$ and $\delta\bar{\mathcal{A}} \equiv \delta\mathcal{A}/(R_{WL}\ell/\pi)$, such that the thermalization effect can be better observed, independently of ℓ.

Let us consider a systematic study on how the thermalization time changes within these geometries. If we want to have a clear comparison with thermalization in the Schwarzschild-AdS case without charge, it is natural to keep fixed the radius of the event horizon, say $r_h = 1$. The mass of the black hole is given by Eq.(30), so we obtain

$$M = 1 + Q^2 \,. \tag{55}$$

This relation between M and Q holds from $Q = 0$ up to the extremal case. From Eq.(31), we find

$$Q_{ext} = \sqrt{\frac{d}{d-2}} \,. \tag{56}$$

Eq.(55) still holds for Q values larger than its extremal value. However, in that case $r_h = 1$ becomes a hidden singularity. The black hole horizon is the larger squared root of the function $U(r)$ as given by Eq.(27). With this choice we can explore the whole parameter range of the problem. The idea is to keep fixed the event horizon radius, and consider the charge in the range $0 \leq Q \leq Q_{ext}$. Then, we will study all the range $0 \leq \mu/T \leq \infty$ in the dual field theory.

This is shown for the two-point functions for different spacetime dimensions $d = 3, 4, 5, 6$ with $\ell = 2, 3, 4$ in Fig. 2 and for the expectation value of rectangular Wilson loops for $\ell = 1, 2, 3$ in Fig. 3. Firstly, we notice certain similarities in comparison with the corresponding Schwarzschild-AdS cases ($Q = 0$). In principle, the thermalization time increases as the separation of the CFT operators at the boundary is increased. Moreover, at a fixed value of the charge, the thermalization time increases as the boundary separation does. For instance, for $\ell = 2$, the renormalized geodesic length practically has no significant differences for the thermalization time for any charge and dimension. However, interestingly, for $\ell = 3$, the differences become more evident, while for $\ell = 4$ RNAdS-BH and AdS-BH cases are notoriously distinct.

One of the most interesting effects we have found is the presence of a swallow-tail pattern near the end of the thermalization process. This phenomenon has been reported earlier in [19] for thermalization of rectangular Wilson loops in AdS_4 having $\mu = 0$, as well as for those

cases when the shell is quasi-stationary. The reason for the emergence of the swallow-tail structure is that, at certain time, there are more than just only one single geodesic minimizing the action. This means that the saddle-point approximation should be taken cautiously. In reference [19], on the other hand, it has been argued that the swallow-tail structure depends on the dimension of the system. However, according to our results displayed in Figs. 2 and 3, this seems to be a universal phenomenon which depends on the penetration of the probes in the bulk interior. In fact, we show how for sufficiently large probes swallow tails are independent on the kind of probe and on the dimension of the asymptotic AdS space. Again, larger dimensions induce smaller variations. This effect is understood by considering that the fraction of the perturbed modes by the shell is smaller as the dimensionality of the system increases.

5 Discussion

In this section we discuss the numerical results obtained by using the formalism developed in the previous sections. We first analyze the results of renormalized geodesic lengths, then minimal area surfaces which are dual to expectation values of rectangular Wilson loops and finally we discuss about the meaning of the swallow tails in the figures. In all the figures corresponding to the geodesic lengths and minimal area surfaces the curves correspond to values of the charge from $Q = 0$ to $Q_{ext} = \sqrt{\frac{d}{d-2}}$, with increments of 0.25. Recall that the mass is given by the relation $M = 1 + Q^2$. The UV cut-off has been taken as $z_0 = 0.01$, we have set $r_h = 1$ and the shell thickness is $v_0 = 0.01$.

Figure 2 shows the results of thermalization with a chemical potential for different spacetime dimensions indicated as AdS_{d+1}, with $d + 1 = 4$, 5, 6 and 7. In all these cases we consider two-point functions as extensive probes. As an example we show three different values of the boundary separation ℓ =2, 3 and 4. The pictures are displayed in such a way that ℓ varies horizontally, while the spacetime dimension changes in the vertical direction. In every picture the vertical axis indicates the renormalized geodesic length as a function of t_0. The fluor-green curve closer to the horizontal axis shows that faster thermalization corresponds to the Schwarzschild-AdS black hole. The rest of curves in all pictures indicates increasing values of the μ/T ratio. Thus, they correspond to thermalization with increasing chemical potential described in terms of Reissner-Nordström AdS_{d+1} black holes. The range of μ/T ratio goes from zero to infinity, and we show several curves where always the fluor-green ones correspond to $\mu/T = 0$ which coincide with the evolution of thermalization reported in reference [20]. As the chemical potential over temperature ratio increases the curves depart from the fluor-green ones, and the larger differences occur for curves corresponding to $\mu/T \to \infty$. Looking at the first column of pictures we observe that for small separation distances of local quantum field theory operators at the boundary, *i.e.* $\ell = 2$, the

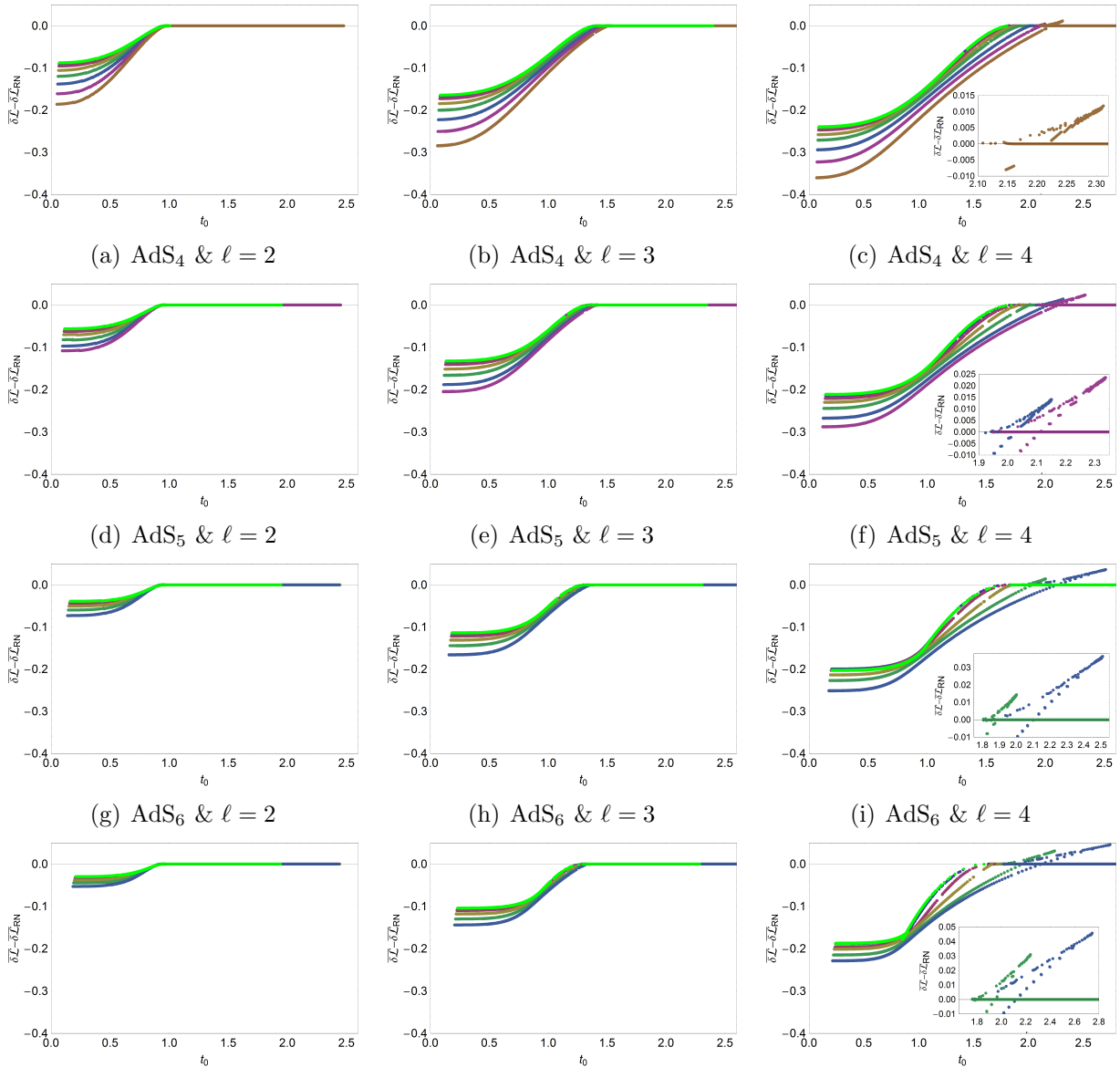

(a) AdS_4 & $\ell = 2$ (b) AdS_4 & $\ell = 3$ (c) AdS_4 & $\ell = 4$

(d) AdS_5 & $\ell = 2$ (e) AdS_5 & $\ell = 3$ (f) AdS_5 & $\ell = 4$

(g) AdS_6 & $\ell = 2$ (h) AdS_6 & $\ell = 3$ (i) AdS_6 & $\ell = 4$

(j) AdS_7 & $\ell = 2$ (k) AdS_7 & $\ell = 3$ (l) AdS_7 & $\ell = 4$

Figure 2: Thermalization of the renormalized geodesic lengths for a RNAdS Vaidya type metric with $d+1 = 4, 5, 6, 7$ and the boundary separation $\ell = 2, 3, 4$. The first curve in each picture (fluor green) indicates the case $Q = 0$, *i.e.* the Schwarzschild-AdS case. The last curve in each case corresponds to the extremal case where $\mu/T \to \infty$. For $\ell = 4$ swallow tails appear before the thermalization takes place. They are shown with more detail in the corresponding insets.

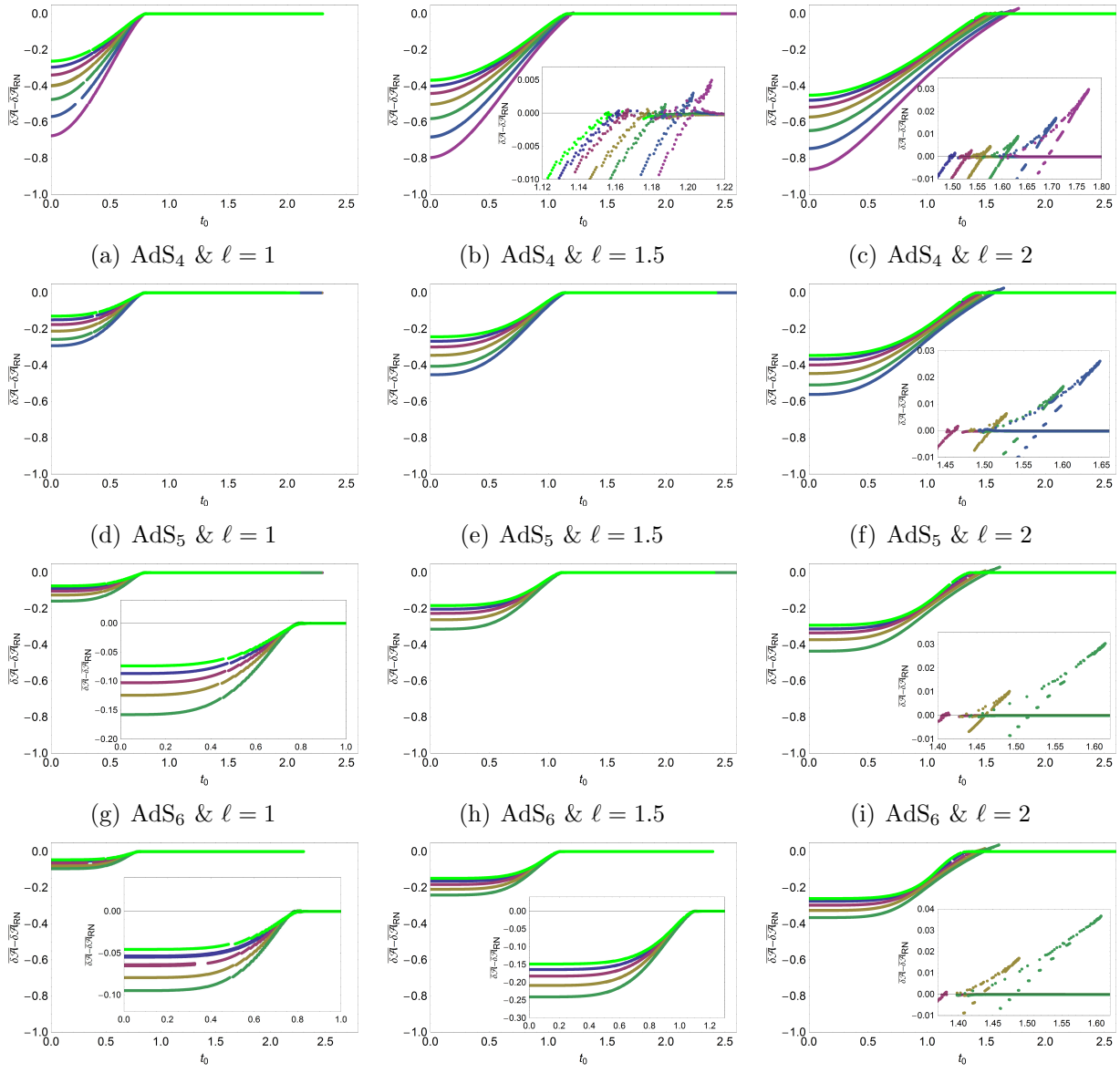

(a) AdS_4 & $\ell = 1$ (b) AdS_4 & $\ell = 1.5$ (c) AdS_4 & $\ell = 2$

(d) AdS_5 & $\ell = 1$ (e) AdS_5 & $\ell = 1.5$ (f) AdS_5 & $\ell = 2$

(g) AdS_6 & $\ell = 1$ (h) AdS_6 & $\ell = 1.5$ (i) AdS_6 & $\ell = 2$

(j) AdS_7 & $\ell = 1$ (k) AdS_7 & $\ell = 1.5$ (l) AdS_7 & $\ell = 2$

Figure 3: Thermalizacion of the renormalized minimal area surfaces for RNAdS Vaidya type metric with $d+1 = 4, 5, 6, 7$, while the boundary separation is $\ell = 1, 1.5, 2$. In each picture the first curve (fluor green) indicates the case $Q = 0$, *i.e.* the Schwarzschild-AdS case. The rest of the curves in each figure correspond to $Q = 0.50, 0.75, \cdots, \sqrt{\frac{d}{d-2}}$. The last case is the extremal where $\mu/T \to \infty$. Insets allow to show the swallow tails in detail. Note that in order to make easier the comparison among different figures the vertical and horizontal scales are kept fixed in all figures.

renormalized geodesic length becomes zero at the same t_0. For $\ell = 3$ (in the second column of pictures) it is already possible to notice a slight enhancement of the thermalization time as μ/T increases. This effect is much more noticeable for $\ell = 4$, in the third column of the pictures. Thus, the conclusion is an enhancement of the thermalization time as the chemical potential over temperature ratio increases, which is more evident as the boundary separation increases.

Figure 3 shows the results of thermalization with a chemical potential for different spacetime dimensions indicated as AdS_{d+1}, with $d+1$ =4, 5, 6 and 7, for minimal area surfaces which turn out to be dual to expectation values of rectangular Wilson loops. Notice that we display values of the boundary separation, $\ell = 1$, 1.5 and 2, which are different from the ones shown in Fig. 2. From the pictures we can see that ℓ varies horizontally, while the spacetime dimension changes in the vertical direction as for the geodesic lengths. In the present case vertical axis indicates the renormalized minimal area surfaces as functions of t_0. The fluor-green curve closer to the horizontal axis shows that faster thermalization corresponds to the Schwarzschild-AdS black hole as before. The curves correspond to thermalization with increasing chemical potential described in terms of Reissner-Nordström AdS_{d+1} black holes. The range of μ/T ratio goes from zero to infinity, and we show several curves where always the fluor-green ones correspond to $\mu/T = 0$. As the chemical potential increases the curves depart from the fluor-green one, and the larger differences occur for curves corresponding to $\mu/T \to \infty$. Thermalization time is obtained when the curves reach zero. For $\ell = 1.5$ (in the second column of pictures) it is already possible to notice a slight enhancement of the thermalization time as μ/T increases. This effect is more noticeable for $\ell = 2$. Therefore, we arrive to the same conclusion as in the geodesic lengths case: there is an enhancement of the thermalization time as the chemical potential over temperature ratio increases, which is more evident as the boundary separation increases.

Each figure 2(a-l) as well as 3(a-l) shows that the thermalization time for renormalized geodesic lengths and minimal area surfaces increases as μ/T increases, while the dimension of the bulk spacetime $d+1$ and the boundary separation ℓ of two local field theory operators are kept fixed. When considering the three figures for a fixed dimension in each horizontal sequence, there are two effects: one is that the thermalization time increases as the boundary separation does; the second effect is that for small ℓ there are no apparent differences in the thermalization time for any value of μ/T and, moreover, it coincides with the Schwarzschild-AdS black hole case. As long as one increases ℓ (see figures 2 and 3 (c, f, i, l)), the thermalization is significantly delayed as μ/T increases. This effect is understood as a consequence of the fact that the term proportional to the charge in $f_{RN}(v, z)$ has opposite relative sign with respect to the term proportional to the mass, so the chemical potential somehow produces an effect similar to the one obtained from the reduction of the black hole mass. In addition, it turns out that the thermalization time is slightly larger for expectation values of rectangular Wilson loops compared with two-point functions. For the same

separation length in the boundary, the minimal area surface dual to the expectation values of Wilson loops penetrate more into the bulk, thus resulting in a more extensive probe of thermalization, which takes more time to measure thermal equilibrium. From the dual quantum field theory side, we expect that the system after receiving a sudden injection of energy and particles will be far from thermal equilibrium. We assume that its dynamics should be controlled by a strongly coupled Yang Mills theory. The study of the thermalization process cannot be done in terms of the hydrodynamic approximation, and therefore, the description of the process is a very hard problem. On the other hand, we can think of a rather intuitive argument, which although has obviously not the value of any rigorous proof, it may help to understand whether our results obtained using a holographic dual model of thermalization are qualitatively consistent with the gauge theory expectations. First notice that in order for the system to reach thermal equilibrium it requires both kinetic and chemical equilibration. The former is expected to be faster than the second one. The reason is that chemical equilibration involves additional interactions. This, in principle, might delay the thermalization process in comparison with the situation where no chemical potential is considered.

Also from these figures a swallow-tail pattern emerges. In the insets of the figures we zoom in the corresponding regions of the figures in order to see the swallow-tail structure in more detail. Now, let us consider the figures for a fixed ℓ. So, increasing the AdS dimension we observe that the effects of chemical potential become less relevant in all cases. This is due to the fact that a geodesic is a one-dimensional line which is not able to account for the effect of other orthogonal space dimensions. Thus, if we increase $d+1$, in order to observe the effect on the thermalization time, we have to use an extended probe having more space dimensions. This effect can be seen by comparison with the thermalization curves using the dual of expectation values of Wilson loops as extended probes. In all the figures we can observe that UV degrees of freedom thermalize first.

It is interesting to analyze the cause of the swallow-tail emergence in thermalization curves with large boundary separation distance. In general this kind of effect is found in systems where there are two different scales. In the present case, there are different length scales that could, in principle, induce the swallow-tail pattern. For instance, the AdS radius, the inverse of confinement temperature T_c, the UV cut-off z_0 and the shell thickness, can all introduce a second scale to the problem. However, we do not find that any of these scales are relevant for the appearance of a swallow tail. In fact, we will show that different solutions given in the swallow tails are actually non-physical solutions of our problem, in the sense that they have not to be taken into account. This can be shown by looking at how the solutions that appear in the swallow tail are. As an example, we show in Fig. 4 these solutions for the swallow tail that appear when evaluating expectation values of rectangular Wilson loops in the extremal RNAdS$_4$ Vaidya metric. What we can appreciate is that from the three different solutions that generate the swallow tail at a certain time, two of them have $z(x)$ functions that propagate inside the event horizon. One could nevertheless think that the appearance

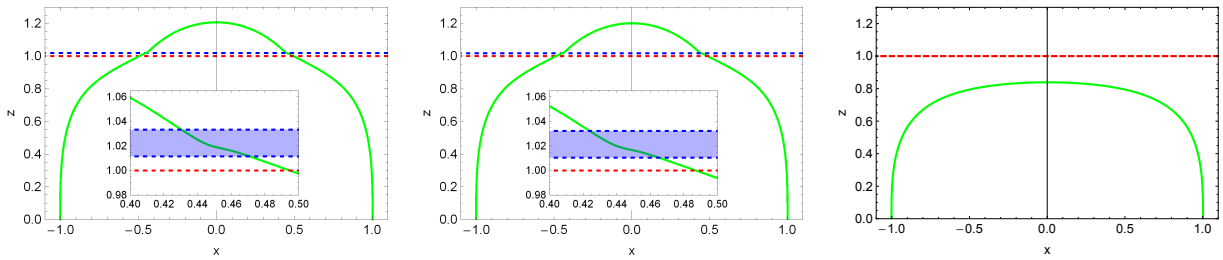

(a) $z_* = 1.207$ & $v_* = -0.194$ (b) $z_* = 1.201$ & $v_* = -0.189$ (c) $z_* = 0.839$ & $v_* = 0.173$

Figure 4: Three different solutions that appear as part of the swallow tail in thermalization of expectation values of Wilson loops in the extremal RNAdS Vaidya geometry with $d = 3$. Time corresponds to $t_0 = 1.778$ in all three cases and separation length is $\ell = 2$. The red dashed line corresponds to the event horizon ($z_h = 1$), while the blue dashed one is the position of the shell. In the first two cases, the shell is located inside the event horizon but still have solutions inside. In the insets we take a closer look at the region near the horizon and consider the shell thickness ($-0.02 \leq v \leq 0.02$) in blue.

of those solutions is due to the shell thickness that can emulate a black hole solution with a deeper event horizon. However, as it is shown in the insets of Figs. 4(a) and 4(b) even by considering the shell thickness we obtain that these solutions propagate beyond the event horizon. So, only the third one, that appears in Fig. 4(c), is the physical and thermalized solution.

The effective model presented above is based on a double quench (for the mass and charge) and it has a metric which evolves in time. These features make, in principle, difficult to think of finding a top-down description from string theory and M-theory. However, it is certainly interesting to study this kind of models based on a collapsing shell of charged dust since it allows to study the thermalization process in a dual strongly coupled quantum field theory. One of the important results is that by using this geometric extended probes one finds a top-down thermalization regardless of the dimension of the AdS space and of whether the shell is charged or not. This is a consequence of the geometric setup, where for smaller boundary separations the dual geometric structures probe a region closer to the boundary. Also, as it is the case for Schwarzschild-AdS black holes there is a delay in the beginning of the thermalization process due to the fact that the system only feels the sudden energy injection at the boundary at distances of its thermal wavelength. We have carried out a systematic investigation by exploring the whole range of μ/T, the boundary separation and the dimension of the AdS spaces. Except for the case of the BTZ black hole the expressions require to solve them numerically. The reason to include chemical potential, using the grand canonical ensemble, is because realistic systems such as QGPs and condensed matter systems have that. In order to do so, the formalism presented in this work, studying a general Reissner-Nordström-AdS black hole Vaidya-type metric in arbitrary number of dimensions,

is very interesting and we hope it will motivate further studies and extensions. In all the cases studied the effect produced by the chemical potential is the delay of the thermalization process, being it more evident as the boundary separation increases. This also agrees with the conclusion that the thermalization of more energetic modes proceeds first in strongly coupled systems.

Acknowledgments

We thank Esteban Calzetta, Nicolás Grandi, Carlos Núñez and Guillermo Silva for useful discussions and Carlos Núñez for a careful reading of the manuscript. This work has been partially supported by the CONICET, the ANPCyT-FONCyT Grant PICT-2007-00849, and the PIP-2010-0396 Grant.

A On null vectors and energy conditions of the RN-AdS-Vaidya type metric

In this Appendix we show how the energy conditions are satisfied for a RN-AdS-Vaidya type metric like the one that has been analyzed in this work as a gravitational dual to thermalization of field theories at finite temperature with a finite chemical potential.

The energy-momentum tensor $T_{\mu\nu}$ at each point of a manifold satisfies the so-called weak-energy condition [54], $T_{\mu\nu}W^\mu W^\nu \geq 0$ for any time-like vector W^μ. In particular, for any null vector N^μ, this becomes the condition $T_{\mu\nu}N^\mu N^\nu \geq 0$. In the case of the Vaidya metric we will follow [16] and consider normal null vectors to surfaces that preserve translation invariance in the boundary coordinates x_i; that is, surfaces of constant v and z. The resulting null vectors are

$$N_1^\mu = \left(0, \frac{z^2}{R^4}, \mathbf{0}\right), \tag{57}$$

$$N_2^\mu = \left(R^2, -\frac{f_{RN}(v,z)}{2}, \mathbf{0}\right), \tag{58}$$

where we have restored units of AdS radius R. With this choice the metric and f_{RN} becomes

$$ds^2 = \frac{1}{z^2}\left[-f_{RN}(v,z)dv^2 - 2R^2 dz dv + R^2 d\mathbf{x^2}\right] \tag{59}$$

$$f_{RN}(v,z) = R^2 - m(v)\frac{z^d}{R^{2d-4}} + q(v)^2\frac{z^{2d-2}}{R^{4d-8}}\,. \tag{60}$$

The normalization has been chosen such that $N_1 \cdot N_2 = -1$. As the only non-vanishing component of the energy-momentum tensor is

$$8\pi G^{d+1}T_{vv} = \frac{(d-1)z^{d-1}}{R^{4d-6}}\left(\frac{1}{2}R^{2d-4}\dot{m}(v) - z^{d-2}q(v)\dot{q}(v)\right), \tag{61}$$

the null energy condition for N_1 is satisfied trivially. For N_2 the energy condition depends on the relation between $m(v)$ and $q(v)$. As mentioned before, for $q(v) = 0$ the condition is always satisfied provided that $\dot{m}(v)$ is non-negative. In the charged case, the expression can be analyzed in a simpler way by making use of the relation between mass, charge and event horizon radius given in Eq.(30). The chosen quenches satisfy

$$m(v) = \frac{M}{2}g(v)\,, \tag{62}$$

$$q(v) = \frac{Q}{2}g(v)\,, \tag{63}$$

where $g(v) = 2\theta(v)$ in the zero shell thickness case and $g(v) = 1 + \tanh(\frac{v}{v_0})$ in the general case. The null energy condition becomes

$$\frac{d-1}{4}\frac{z^{d-1}}{R^{4d-10}}\dot{g}(v)\left(\frac{R^{4d-6}}{z_h^d} + Q^2\left(z_h^{d-2} - z^{d-2}g(v)\right)\right) \geq 0\,. \tag{64}$$

The overall function $\dot{g}(v)$ makes that the condition is satisfied if

$$z \leq \frac{1}{g(v)^{\frac{1}{d-2}}} \left(\frac{z_h^{-d} R^{4d-6}}{Q^2} + z_h^{d-2} \right)^{\frac{1}{d-2}} . \tag{65}$$

For the zero shell thickness, i.e. for the step function, the null energy condition is satisfied for any value of v. In the case of a smoother function, there can be a small region for large Q around $v = 0$, where the condition is not satisfied. On the other hand, we can always consider R and z_h to be within a parametric region where $R^{4d-6}/z_h^{2d-2} \geq Q^2$, where the null energy condition is satisfied for any value of v. In addition, as the limit case of zero shell thickness is indeed physical, we consider that it is interesting to study the whole range of parameters from zero charge to the extremal case.

References

[1] E. Shuryak, "Why does the quark gluon plasma at RHIC behave as a nearly ideal fluid?," Prog. Part. Nucl. Phys. **53** (2004) 273 [arXiv:hep-ph/0312227].

[2] J. Schukraft and f. t. A. Collaboration, "First Results from the ALICE experiment at the LHC," arXiv:1103.3474 [hep-ex].

[3] N. Armesto *et al.*, "Heavy Ion Collisions at the LHC - Last Call for Predictions," J. Phys. G **35** (2008) 054001 [arXiv:0711.0974 [hep-ph]].

[4] J. M. Maldacena, "The large N limit of superconformal field theories and supergravity," Adv. Theor. Math. Phys. **2** (1998) 231 [Int. J. Theor. Phys. **38** (1999) 1113] [arXiv:hep-th/9711200].

[5] S. S. Gubser, I. R. Klebanov and A. M. Polyakov, "Gauge theory correlators from non-critical string theory," Phys. Lett. B **428** (1998) 105 [arXiv:hep-th/9802109].

[6] E. Witten, "Anti-de Sitter space and holography," Adv. Theor. Math. Phys. **2** (1998) 253 [arXiv:hep-th/9802150].

[7] G. Policastro, D. T. Son and A. O. Starinets, "The Shear viscosity of strongly coupled N=4 supersymmetric Yang-Mills plasma," Phys. Rev. Lett. **87** (2001) 081601 [hep-th/0104066].

[8] J. Casalderrey-Solana, H. Liu, D. Mateos, K. Rajagopal and U. A. Wiedemann, "Gauge/String Duality, Hot QCD and Heavy Ion Collisions," arXiv:1101.0618 [hep-th].

[9] A. Buchel, J. T. Liu and A. O. Starinets, "Coupling constant dependence of the shear viscosity in N=4 supersymmetric Yang-Mills theory," Nucl. Phys. B **707** (2005) 56 [hep-th/0406264].

[10] G. Policastro, D. T. Son and A. O. Starinets, "From AdS / CFT correspondence to hydrodynamics," JHEP **0209** (2002) 043 [hep-th/0205052].

[11] B. Hassanain and M. Schvellinger, "Towards 't Hooft parameter corrections to charge transport in strongly-coupled plasma," JHEP **1010** (2010) 068 [arXiv:1006.5480 [hep-th]].

[12] B. Hassanain and M. Schvellinger, "Plasma conductivity at finite coupling," JHEP **1201** (2012) 114 [arXiv:1108.6306 [hep-th]].

[13] S. Caron-Huot, P. Kovtun, G. D. Moore, A. Starinets and L. G. Yaffe, "Photon and dilepton production in supersymmetric Yang-Mills plasma," JHEP **0612** (2006) 015 [hep-th/0607237].

[14] B. Hassanain and M. Schvellinger, "Diagnostics of plasma photoemission at strong coupling," arXiv:1110.0526 [hep-th].

[15] S. R. Das, T. Nishioka and T. Takayanagi, "Probe Branes, Time-dependent Couplings and Thermalization in AdS/CFT," JHEP **1007** (2010) 071 [arXiv:1005.3348 [hep-th]].

[16] J. Abajo-Arrastia, J. Aparicio and E. Lopez, "Holographic Evolution of Entanglement Entropy," JHEP **1011** (2010) 149 [arXiv:1006.4090 [hep-th]].

[17] T. Albash and C. V. Johnson, "Evolution of Holographic Entanglement Entropy after Thermal and Electromagnetic Quenches," New J. Phys. **13** (2011) 045017 [arXiv:1008.3027 [hep-th]].

[18] H. Ebrahim and M. Headrick, "Instantaneous Thermalization in Holographic Plasmas," arXiv:1010.5443 [hep-th].

[19] V. Balasubramanian, A. Bernamonti, J. de Boer, N. Copland, B. Craps, E. Keski-Vakkuri, B. Muller and A. Schafer *et al.*, "Thermalization of Strongly Coupled Field Theories," Phys. Rev. Lett. **106** (2011) 191601 [arXiv:1012.4753 [hep-th]].

[20] V. Balasubramanian, A. Bernamonti, J. de Boer, N. Copland, B. Craps, E. Keski-Vakkuri, B. Muller and A. Schafer *et al.*, "Holographic Thermalization," Phys. Rev. D **84** (2011) 026010 [arXiv:1103.2683 [hep-th]].

[21] D. Garfinkle and L. A. Pando Zayas, "Rapid Thermalization in Field Theory from Gravitational Collapse," Phys. Rev. D **84** (2011) 066006 [arXiv:1106.2339 [hep-th]].

[22] J. Aparicio and E. Lopez, "Evolution of Two-Point Functions from Holography," JHEP **1112** (2011) 082 [arXiv:1109.3571 [hep-th]].

[23] A. Allais and E. Tonni, "Holographic evolution of the mutual information," JHEP **1201** (2012) 102 [arXiv:1110.1607 [hep-th]].

[24] V. Keranen, E. Keski-Vakkuri and L. Thorlacius, "Thermalization and entanglement following a non-relativistic holographic quench," Phys. Rev. D **85** (2012) 026005 [arXiv:1110.5035 [hep-th]].

[25] D. Garfinkle, L. A. Pando Zayas and D. Reichmann, "On Field Theory Thermalization from Gravitational Collapse," JHEP **1202** (2012) 119 [arXiv:1110.5823 [hep-th]].

[26] S. R. Das, "Holographic Quantum Quench," J. Phys. Conf. Ser. **343** (2012) 012027 [arXiv:1111.7275 [hep-th]].

[27] V. E. Hubeny, "Extremal surfaces as bulk probes in AdS/CFT," arXiv:1203.1044 [hep-th].

[28] U. H. Danielsson, E. Keski-Vakkuri and M. Kruczenski, "Black hole formation in AdS and thermalization on the boundary," JHEP **0002** (2000) 039 [hep-th/9912209].

[29] S. B. Giddings and S. F. Ross, "D3-brane shells to black branes on the Coulomb branch," Phys. Rev. D **61** (2000) 024036 [hep-th/9907204].

[30] R. A. Janik and R. B. Peschanski, "Gauge/gravity duality and thermalization of a boost-invariant perfect fluid," Phys. Rev. D **74** (2006) 046007 [hep-th/0606149].

[31] R. A. Janik, "Viscous plasma evolution from gravity using AdS/CFT," Phys. Rev. Lett. **98** (2007) 022302 [hep-th/0610144].

[32] P. M. Chesler and L. G. Yaffe, "Horizon formation and far-from-equilibrium isotropization in supersymmetric Yang-Mills plasma," Phys. Rev. Lett. **102** (2009) 211601 [arXiv:0812.2053 [hep-th]].

[33] P. M. Chesler and L. G. Yaffe, "Boost invariant flow, black hole formation, and far-from-equilibrium dynamics in N = 4 supersymmetric Yang-Mills theory," Phys. Rev. D **82** (2010) 026006 [arXiv:0906.4426 [hep-th]].

[34] S. Bhattacharyya and S. Minwalla, "Weak Field Black Hole Formation in Asymptotically AdS Spacetimes," JHEP **0909** (2009) 034 [arXiv:0904.0464 [hep-th]].

[35] S. Lin and E. Shuryak, "Toward the AdS/CFT Gravity Dual for High Energy Collisions. 3. Gravitationally Collapsing Shell and Quasiequilibrium," Phys. Rev. D **78** (2008) 125018 [arXiv:0808.0910 [hep-th]].

[36] J. Adams *et al.* [STAR Collaboration], "Experimental and theoretical challenges in the search for the quark gluon plasma: The STAR Collaboration's critical assessment of the evidence from RHIC collisions," Nucl. Phys. A **757** (2005) 102 [nucl-ex/0501009].

[37] B. B. Back, M. D. Baker, M. Ballintijn, D. S. Barton, B. Becker, R. R. Betts, A. A. Bickley and R. Bindel *et al.*, "The PHOBOS perspective on discoveries at RHIC," Nucl. Phys. A **757** (2005) 28 [nucl-ex/0410022].

[38] K. Adcox *et al.* [PHENIX Collaboration], "Formation of dense partonic matter in relativistic nucleus-nucleus collisions at RHIC: Experimental evaluation by the PHENIX collaboration," Nucl. Phys. A **757** (2005) 184 [nucl-ex/0410003].

[39] I. Arsene *et al.* [BRAHMS Collaboration], "Quark gluon plasma and color glass condensate at RHIC? The Perspective from the BRAHMS experiment," Nucl. Phys. A **757** (2005) 1 [nucl-ex/0410020].

[40] R. C. Myers, M. F. Paulos and A. Sinha, "Holographic Hydrodynamics with a Chemical Potential," JHEP **0906** (2009) 006 [arXiv:0903.2834 [hep-th]].

[41] C. Martinez, C. Teitelboim and J. Zanelli, "Charged rotating black hole in three space-time dimensions," Phys. Rev. D **61** (2000) 104013 [hep-th/9912259].

[42] G. Grignani, T. Harmark, A. Marini, N. A. Obers and M. Orselli, "Thermal string probes in AdS and finite temperature Wilson loops," arXiv:1201.4862 [hep-th].

[43] S. Ryu and T. Takayanagi, "Holographic derivation of entanglement entropy from AdS/CFT," Phys. Rev. Lett. **96** (2006) 181602 [hep-th/0603001].

[44] S. Ryu and T. Takayanagi, "Aspects of Holographic Entanglement Entropy," JHEP **0608** (2006) 045 [hep-th/0605073].

[45] T. Nishioka, S. Ryu and T. Takayanagi, "Holographic Entanglement Entropy: An Overview," J. Phys. A A **42** (2009) 504008 [arXiv:0905.0932 [hep-th]].

[46] P. C. Vaidya, "The external field of a radiating star in general relativity", Curr. Sci. **12** (1943) 183.

[47] P. C. Vaidya, "The gravitational field of a radiating star", Proc. Indian. Acad. Sci. A. **33** (1951) 264

[48] V. Balasubramanian and S. F. Ross, "Holographic particle detection," Phys. Rev. D **61** (2000) 044007 [hep-th/9906226].

[49] A. Chamblin, R. Emparan, C. V. Johnson and R. C. Myers, "Charged AdS black holes and catastrophic holography," Phys. Rev. D **60** (1999) 064018 [hep-th/9902170].

[50] A. Chamblin, R. Emparan, C. V. Johnson and R. C. Myers, "Holography, thermodynamics and fluctuations of charged AdS black holes," Phys. Rev. D **60** (1999) 104026 [hep-th/9904197].

[51] R. Emparan, "AdS membranes wrapped on surfaces of arbitrary genus," Phys. Lett. B **432** (1998) 74 [hep-th/9804031].

[52] J. M. Maldacena, "Wilson loops in large N field theories," Phys. Rev. Lett. **80** (1998) 4859 [hep-th/9803002].

[53] S. -J. Rey and J. -T. Yee, "Macroscopic strings as heavy quarks in large N gauge theory and anti-de Sitter supergravity," Eur. Phys. J. C **22** (2001) 379 [hep-th/9803001].

[54] S. W. Hawking and G. F. R. Ellis, "The Large scale structure of space-time," Cambridge University Press, Cambridge, 1973.